SCIENTIFIC REPORTS

OPEN

Structural Evolution of Chemically-Driven RuO_2 Nanowires and 3-Dimensional Design for Photo-Catalytic Applications

Received: 11 November 2014
Accepted: 26 May 2015
Published: 07 July 2015

Joonmo Park[1], Jae Won Lee[1], Byeong Uk Ye[1], Sung He Chun[2], Sang Hoon Joo[3], Hyunwoong Park[4], Heon Lee[5], Hu Young Jeong[6], Myung Hwa Kim[2] & Jeong Min Baik[1]

Growth mechanism of chemically-driven RuO_2 nanowires is explored and used to fabricate three-dimensional RuO_2 branched Au-TiO_2 nanowire electrodes for the photostable solar water oxidation. For the real time structural evolution during the nanowire growth, the amorphous RuO_2 precursors ($Ru(OH)_3 \cdot H_2O$) are heated at 180˚C, producing the RuO_2 nanoparticles with the tetragonal crystallographic structure and Ru enriched amorphous phases, observed through the in-situ synchrotron x-ray diffraction and the high-resolution transmission electron microscope images. Growth then proceeds by Ru diffusion to the nanoparticles, followed by the diffusion to the growing surface of the nanowire in oxygen ambient, supported by the nucleation theory. The RuO_2 branched Au-TiO_2 nanowire arrays shows a remarkable enhancement in the photocurrent density by approximately 60% and 200%, in the UV-visible and Visible region, respectively, compared with pristine TiO_2 nanowires. Furthermore, there is no significant decrease in the device's photoconductance with UV-visible illumination during 1 day, making it possible to produce oxygen gas without the loss of the photoactvity.

Three-dimensional (3D) branched nanowire arrays have received much attention owing to their peculiar and interesting optical, electronic, and catalytic properties[1–3]. Because of their very high surface-to-volume ratios, the direct conduction pathway for charge transport, and the low light reflectance, the 3D nanostructures can in principle are used to create very practical nanophotonic devices such as photochemical cells, sensors, light-emitting diodes, and solar cells[3–5].

Ruthenium dioxide (RuO_2) are of great interest as a promising candidate as electrodes in electrochemical devices and active catalysts due to extremely low resistivity, excellent chemical and thermal stability, catalytic property[6,7]. In particular, it is well-known to be among the most efficient electrocatalysts for the oxygen evolution reaction (OER) in alkaline and acid electrolytes, promoting the photoelectrochemical (PEC) water oxidation in photochemical cells. The sluggish anodic OER as well as the predominant absorption in the UV region may be a main factor in determining the capability of the titanium dioxide (TiO_2)-based photoelectrodes[8]. Recently, the IrO_2/hemin-coated TiO_2 nanowires showed much enhanced

[1]School of Materials Science and Engineering, KIST-UNIST-Ulsan Center for Convergent Materials, Ulsan National Institute of Science and Technology (UNIST), Ulsan 689-798, Republic of Korea. [2]Department of Chemistry & Nano Science, Global Top 5 Program, Ewha Womans University, Seoul 120-745, Republic of Korea. [3]School of Energy & Chemical Engineering Department of Chemistry Ulsan National Institute of Science & Technology (UNIST), Ulsan 689-798, Republic of Korea. [4]School of Energy Engineering, Kyungpook National University, Daegu 702–701, Republic of Korea. [5]Department of Materials Science and Engineering, Korea University, Anam-dong 5-ga, Seongbuk-gu, Seoul 136-713, Republic of Korea. [6]UNIST Central Research Facilities (UCRF), Ulsan National Institute of Science and Technology (UNIST), Ulsan 689-798, Republic of Korea. Correspondence and requests for materials should be addressed to J.M.B. (email: jbaik@unist.ac.kr)

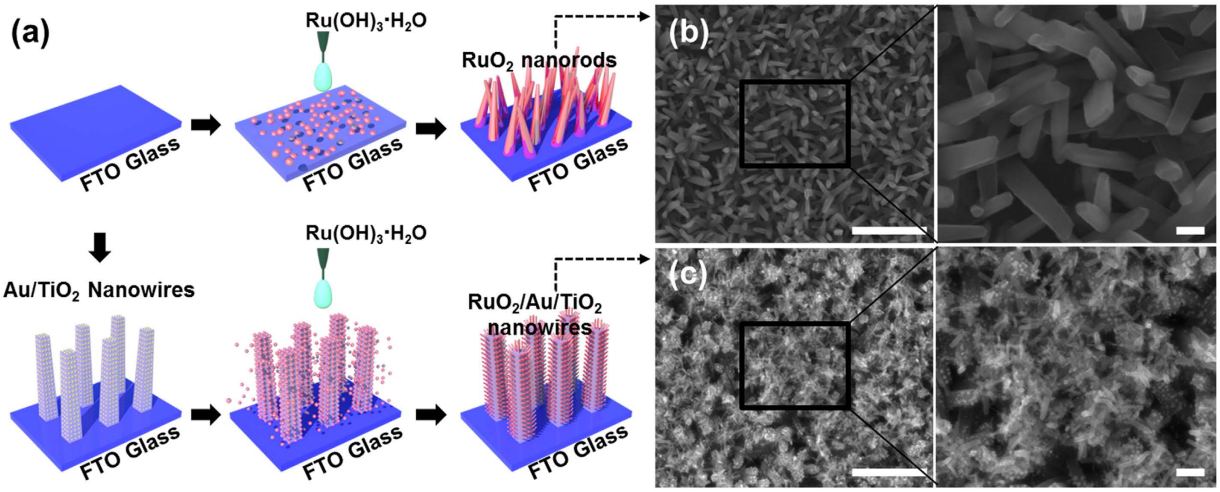

Figure 1. (**a**) Schematic diagram for the fabrication of RuO_2 nanowires and 3D RuO_2 branched Au-TiO_2 nanostructure, (**b**,**c**) top-view SEM images of RuO_2 nanowires and 3D branched nanostructures (scale bars in the left and right images, 1 μm and 100 nm, respectively).

photocurrent with ~100% increase compared to the pristine TiO_2 nanowires[9]. The photocatatytic activities of $TiSi_2$/graphene nanoparticles and Nb/N-doped anatase TiO_2 nanoparticles were reported to be improved by the loading of RuO_2 nanoparticles[10,11]. Also, the RuO_2-Au composites enhanced the catalytic property with ~30% than pure Au[12]. Thus, most of the catalysts are formed as a form of fine nanoparticles. The photocatalytic activity may be enhanced by the advantages imparted by the 3D branched nanostructure, as mentioned above. Furthermore, since 2012, it is also interesting that the price of Ru has decreased by approximately 40% on sales in Asia and U.S.[13].

In spite of its great potential toward future real applications, on the other hand, the growth of highly single crystalline RuO_2 nanowires has been recently reported by thermal oxidation or chemical vapor deposition (CVD) of appropriate Ru-based precursors and reactive sputtering using pure Ru metal targets[7,14,15]. However, it is still challenging to make RuO_2 nanowires with well-defined crystal structures with desirable density in real applications. For the RuO_2 nanowires grown by a CVD, a process referred to as vapor-solid (VS) growth model was suggested via the formation of gaseous RuO_4 species which is a highly volatile and very low melting point intermediate[14]. A thermal conversion from amorphous oxides nanoparticle precursor was also suggested to synthesize single crystalline nanowires of oxide materials[15]. However, it is necessary to explore this mechanism in greater detail in order to fully demonstrate the preferential and unidirectional crystal growth of RuO_2.

Here, we focus on the real-time structural evolution of chemically-driven RuO_2 nanowires for the growth mechanism and report a facile method to fabricate RuO_2 branched Au-TiO_2 nanowire arrays for the photostable solar water oxidation. The in-situ synchrotron x-ray diffraction (in-situ SXRD) shows the direct transition of the amorphous RuO_2 precursors ($Ru(OH)_3{\cdot}H_2O$) to crystalline RuO_2 nanoparticles with the tetragonal crystallographic structure at 180 °C, without the intermediate change formation. In the high-resolution transmission electron microscope (HRTEM), we find that most of the crystallized nanoparticles are in the vicinity of the nanowires and the amorphous region is Ru enriched by about 10% in comparison to the RuO_2 nanowire. This means that the growth proceeds by Ru diffusion to the nanoparticles, increasing the size of the nanoparticles, eventually, forming the nanowires. At low temperature less than 250 °C, the diffusion is so slow, thereby, the nanowires are very short (less than 1 μm at the growth time of several hours). We believe that this process is supported by the nucleation theory. We also carefully explore the photocatalytic performance of the water splitting of the branched nanowires and the performance is compared with pristine TiO_2 nanowires. We found that the photoactivity was effectively enhanced in the entire UV-visible region, especially more effective in visible light, due to the high catalytic properties of the RuO_2 for the water oxidation and the efficient plasmonic absorption with efficient charge separation to TiO_2 and Au interface, catalyzing the oxygen evolution of the 3D RuO_2 branched structure on the Au surface. The electrodes were quite stable during long-term use (we believe that it may ascribe to the high-crystalline properties of the RuO_2 nanowires).

Results and Discussion

The schematic diagrams outlining the fabrication process of 1D RuO_2 nanowires and 3D RuO_2 branched Au-TiO_2 nanowires are shown in Fig. 1a and detailed information described in Experimental section. Scanning electron microscopy (SEM) images in Fig. 1b shows the product (of a reaction carried out at 250 °C) to consist of long, randomly oriented RuO_2 nanowires without any catalyst particles at the end of their tips. The nanowires (0.5 ~ 1 μm long and 130 ~ 170 nm in diameter) grow out of the

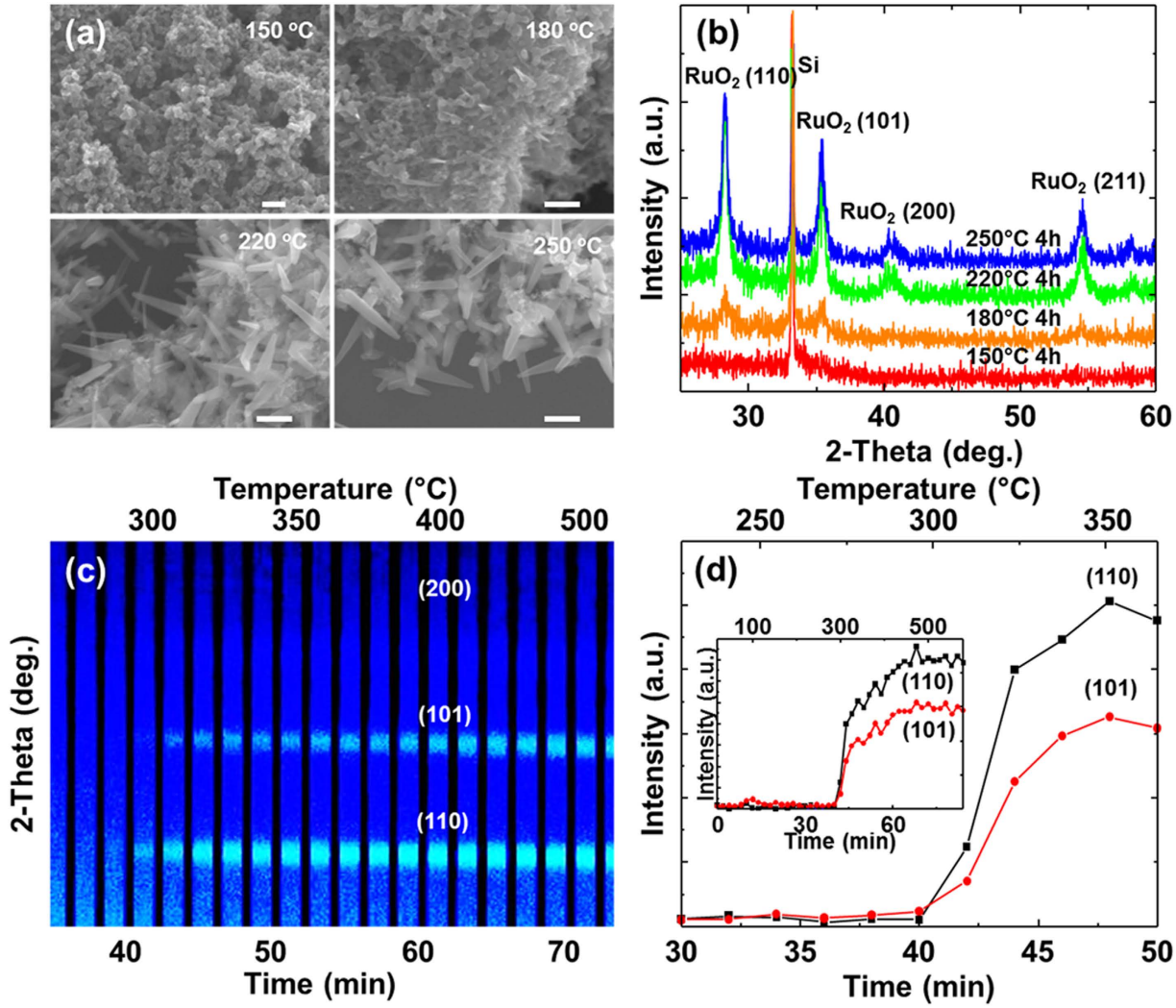

Figure 2. (**a**) SEM images and (**b**) the corresponding XRD patterns (● : (110), ○ : (101), ■ : (200), and □ : (211)) of RuO_2 nanowires as a function of temperature (scale bar, 100 nm). The peak at 33.2° is due to the substrate. (**c**) The in-situ synchrotron radiation diffraction from the growth of RuO_2 nanowires as the temperature increases to 150 ~ 600 °C. Each vertical line is one XRD scan, with the intensity represented by the color. The first scan is at the left, and time progresses right. (**d**) The change in the intensity of (101) and (110) plane with time and inset image is full time.

plane of the substrate in the rectangular shape. Figure 1c shows RuO_2 nanowires directly grown on hydrothermally-grown TiO_2 nanowires with Au nanoparticles (AuNPs), producing 3D branched nanowires. The lengths of most of the nanowires fall in the range 60 ~ 80 nm. The mean nanowire width was determined to be 25 nm. The smaller RuO_2 nanowires in the 3D branched structures ascribes to the decrease in the amount of the precursor, which is an important factor in determining the length and width of the nanowires.

Figure 2a shows SEM images of the as-grown RuO_2 nanowires on a Si substrate synthesized by heating the RuO_2 precursors in air atmosphere in the range of 150 ~ 250 °C during 4 hrs. At low temperature less than 150 °C, only nanoparticles were observed and there were no nanowires on the substrates. In ex-situ x-ray diffraction (XRD), there are no peaks in the spectra, meaning that the nanoparticles are still amorphous. As the temperature increases to 180 °C, three peaks corresponding to the (110), (101), and (211) planes were clearly observed, confirming that the amorphous nanoparticles start to be crystallized at the temperature. In the SEM image, many straight nanowires with apparent tapering at the end and without any cluster at the tip were also seen. Further increase in the temperature enhances the growth of the nanowires, increasing the intensity of the three peaks, and produces additional peak corresponding to the (200) plane. At 250 °C, the length and diameter of the nanowires are in the range of 150 nm and 18 nm, respectively. The length and diameter of the nanowires increase as the temperature increases, while the aspect ratio decreases with the temperature (Supplementary Fig. S1).

In order to further investigate the synthetic process, such as intermediate phase formation over annealing time and temperature, in-situ SXRD experiments were carefully performed in the course of the growth process. In-situ SXRD data provides direct identification of the solids and a sequence of events in the formation of different objects and their growth. The ruthenium hydroxide precursors are put on the stages and then heated by external power sources up to 600 °C with the ramping speed of 7 °C/min. 42 data points for 2 minutes at each temperature interval were obtained. However, experience tells that the measured temperature is not equal to that of the nanoparticles, which will be lower. In the initial stage of the heating, there is no peak. As the temperature increases to about 300 °C, two peaks corresponding to the (110) and (101) planes are observed. However, we could observe any other peaks, indicating the spontaneous growth of the RuO_2 phases from the amorphous phases without any intermediate phase formed.

The above spontaneous growth of the nanowires during the oxidation of precursors without the use of conventional templates or catalysts has received significant attention in the nanotechnology community. The VS model was usually proposed to understand the growth of ZnO and SnO_2 nanowires based on the evaporation of the precursors[16,17]. However, the RuO_2 synthesis is carried out at low temperature of ~180 °C, at which the equilibrium vapor pressures of the pure elements are negligibly small, therefore cannot be ascribed to the model. The growth of the nanowires may ascribe to the diffusion of the cations during the oxidation, forming the tip-like geometry of a single nanowire, in which the driving force for the diffusion is related to the internal stress associated with the phase formation at the CuO/Cu_2O interface. Also, metal-oxides nanowires such as VO_2, V_2O_5, MoO_2, MoO_3, and Fe_3O_4, can be grown via the diffusion and solidification of nanodroplets near the bulk melting point[18–23].

The detailed growth mechanism was characterized by bright-field TEM (BFTEM) and HRTEM images, as shown in Fig. 3. Figure 3a is a BFTEM image of a single nanowire grown at 190 °C with a diameter of approximately 30 nm. The HRTEM image and the corresponding fast-Fourier transformed (FFT) of the nanowire reveal highly ordered lattice fringes, demonstrating that the nanowire is a defect-free single crystal (Fig. 3b). The RuO_2 nanowire has identified as a tetragonal crystalline (110) phase. In the vicinity of the region where the nanowire starts to be grown, there are some crystallized RuO_2 nanoparticles that are ~4 nm in size are clearly seen in the vicinity of the nanowires, while most of the nanoparticles exist as a form of amorphous elsewhere (Fig. 3c,d). Any additional Ru-based crystalline phases except the RuO_2 phase, tetragonal crystallographic structure, are not observed. This implies that the nanowires are grown from the amorphous nanoparticles by the direct recrystallization process.

Previously, it was reported that the amorphous RuO_2 precursors started to lose the water of the hydration to create the anhydrous RuO_2 nanoparticles and Ru metals at 90 °C, as follows[24];

$$4\left[\mathrm{Ru(OH)_3 \bullet} H_2O\right] = 3\mathrm{RuO_2} + \mathrm{Ru} + 10\mathrm{H_2O}$$

The rate of Ru/RuO_2 content was approximately 0.3 in N_2 ambient, meaning that the nanoparticles are amorphous, and increased with the annealing temperature. Actually, it was observed that the amorphous region in Fig. 3c, about 20 nm away from the nanowire, was Ru enriched by about 10% in comparison to the RuO_2 nanowire in Fig. 3b, determined by energy dispersive spectroscopy (EDS). However, most of nanoparticles are seen to be crystalline in the vicinity of the nanowire. The size of the nanoparticles is in the range of 2 ~ 4 nm. According to the nucleation theory, the critical radius (r^*) of the nucleation critically depends on the surface energy (γ), the latent heat of fusion (ΔH_f), the melting temperature (T_m), and the growth temperature (T_g), which is given by,

$$r^* = r_c = \left(\frac{2\gamma}{\Delta H_f}\right)\left(\frac{T_m}{T_m - T_g}\right)$$

Here, the melting temperature and latent heat of fusion are 1200 °C and $1.66 \times 107\,J/m^3$, respectively. The surface free energy of (110) and (001) planes are $1.136\,J/m^2$ and $1.398\,J/m^2$, respectively[24,25]. In this case, the critical thickness of RuO_2 is calculated to be about 2 nm at 190 °C, similar with those observed in the TEM images (Fig. 3d). The observation of the RuO_2 crystalline nanoparticles between the amorphous phase and the nanowire may suggests that the amorphous phase is crystallized before the growth of the nanowires.

The growth rate of the nanowires is mainly limited by the rate of transport of mass, the diffusion rate of Ru and RuO_2 materials produced by the heating process of RuO_2 precursor. The activation energy (ΔE) for the migration of Ru and RuO_2 of ΔE is supposed to be 384 kJ/mol and 3140 kJ/mol, respectively through latent heat of fusion (Ru: 24 kJ/mol, RuO_2: 314 kJ/mol)[26]. This indicates that ΔE of RuO_2 is about 8 times of magnitude of larger than that of Ru, meaning that the diffusion of Ru metals is the dominating process. The concentration gradient of Ru from the amorphous phase to the nanowires promotes the diffusion, enhancing the growth of the nanowires. We also believe that the Ru metals migrate from the bottom to top region of the nanowires through the surface because the bulk diffusion becomes significant at only high temperature. In O_2 ambient, the Ru reacts with oxygen, producing the RuO_2 on the surface[27]. Actually, at free oxygenless atmosphere such as ambient gases such as nitrogen or under vacuum conditions, there are no nanowires on the substrates.

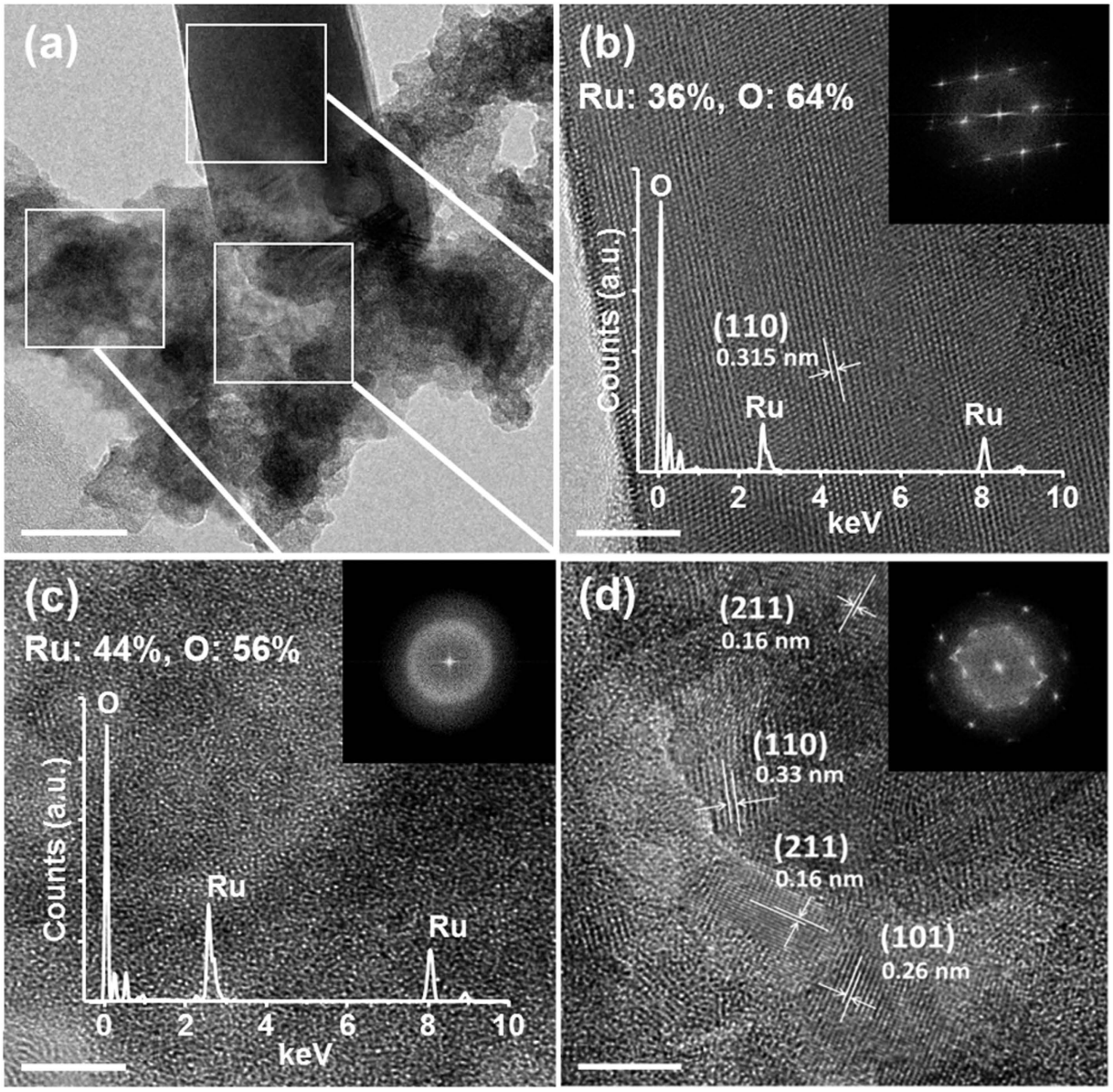

Figure 3. (**a**) BF- TEM image near the bottom of the RuO_2 nanowire (scale bar 20 nm). (**b**) HRTEM image of RuO_2 nanowire obtained after annealing at 190 °C for 1 hr. (**c**) Magnified HRTEM image of amorphous RuO_2 region and (**d**) crystalline RuO_2 nanoparticles at the interface between the region and nanowire (Fig. b, c and d scale bar 5 nm). Inset in (**b**,**c**) show the EDS spectra.

The RuO_2 nanowires were successfully grown on the Au-decorated TiO_2 nanowires, by precisely controlling the concentration of precursors and the growth temperature. HRTEM image in Fig. 4a shows that single-crystalline RuO_2 nanowire is directly grown on the Au nanoparticle. EDS elemental mapping of Fig. 4b clearly also confirms each elemental distribution.

The PEC performance of the TiO_2-based photoelectrodes was examined in a three-electrode configuration with Ag/AgCl as the reference electrode and a Pt wire as the counter electrode. Figure 5a shows the photocurrent-potential characteristics of the TiO_2 nanowires, AuNPs decorated TiO_2 nanowires, and RuO_2 branched AuNPs-TiO_2 nanowires recorded in 0.5 M Na_2SO_4 electrolyte (pH = 7.2) under AM 1.5G illumination of 100 mW/cm^2. The dark scans revealed a small background current of ~2×10^{-3} mA/cm^2, negligible compared to the photocurrent densities of all photoelectrodes. Upon illumination with white light, the pristine TiO_2 nanowires electrodes show a photocurrent density of 0.673 mA/cm^2 at 1.23 V vs. RHE (0.61 V vs. Ag/AgCl). As AuNPs are decorated onto the nanowires, the photocurrent density increases to 0.909 mA/cm^2 at the same potential, associated with the surface plasmonic resonance effect of the AuNPs[28]. It was also observed that under visible-light illumination, the photocurrent density of AuNPs-TiO_2 nanowires was increased by 1.93 times, in comparison with pristine TiO_2 nanowires, obtained by adding a 420 nm long-pass filter to the white source, as shown in Fig. 5b. The formation of

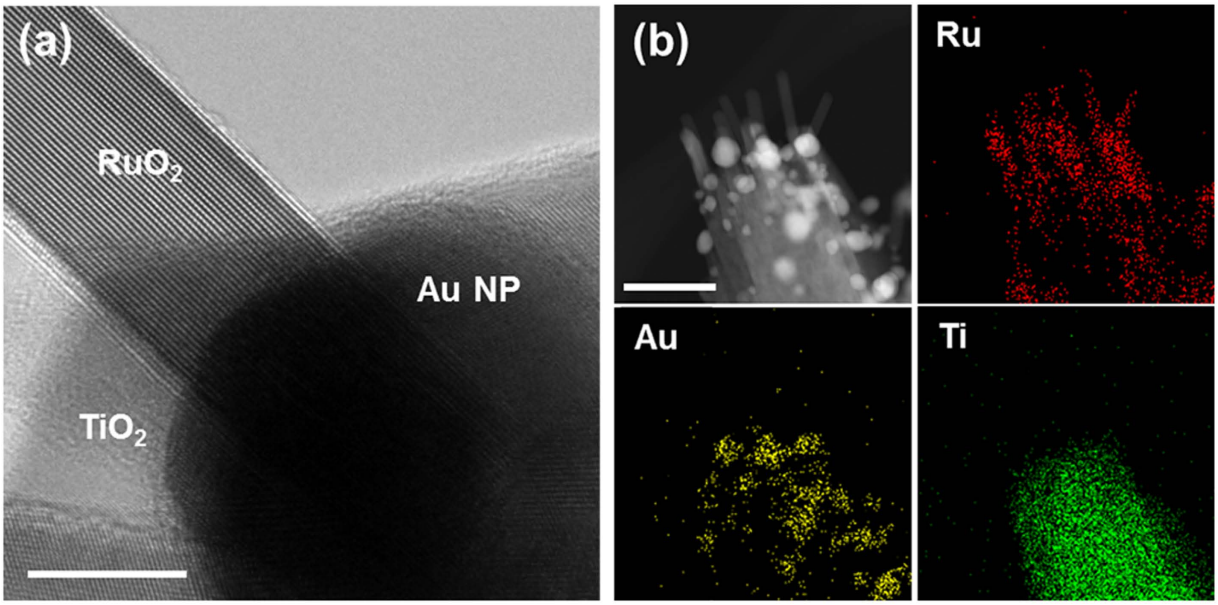

Figure 4. (**a**) TEM image of RuO_2 nanowire on Au nanoparticle-decorated TiO_2 nanowire. It is clearly seen that the nanowire is grown on the Au nanoparticle (scale bar 20 nm). (**b**) High-angle annular dark field (HAADF) scanning TEM image of 3D branched nanowires. EDS elemental distribution map of Ru, Au, and Ti (scale bar 100 nm).

RuO_2 nanowires on AuNPs-TiO_2 nanowires increases the photocurrent density to 1.052 mA/cm^2, around 56% enhancement, compared with pristine TiO_2 nanowires. It is believed that the RuO_2 promotes the electron transfer to the AuNPs due to the high catalytic properties for the water oxidation and the efficient hole injection to RuO_2 to AuNPs, catalyzing the oxygen evolution (Supplementary Fig. S2). This process is prominent seen under visible light. We also observed that the photocurrent of the branched nanowires significantly increased over approximately 0.7 V vs. RHE, compared to that of the AuNPs-TiO_2 nanowires, with a slight shift in the onset voltage. This may be related to the flat band voltage as 0.41 eV of the work function difference between Au and RuO_2. The slight shift in the onset voltage may also be ascribed to the low overpotential on the Au-TiO_2 nanowires associated with the oxygen reduction[29,30].

For the long photostability of the electrodes, the photocurrent was measured under illumination conditions of illuminated with white light at 1.23 V vs. RHE as a function of time up to 24 hrs. Figure 5c shows that the photocurrent decreases slowly up to 24 hrs after a little increase in photocurrent within 3 hrs, which may ascribe to the build-up of hydrogen concentration on Pt electrodes. The rapid decrease in the photocurrent of the efficient photoelectrodes as major limitation to commercialization was not observed here[31], which may ascribe to the highly crystalline properties of the RuO_2 nanowires and the good chemical stability of the TiO_2. Gas chromatographic measurements under the illumination conditions described above also shows that there is no significant difference between the calculated oxygen amount from the photocurrent density and the oxygen evolution amount. This may imply that the RuO_2 branched Au-TiO_2 electrodes has stoichiometric amount reaction for H_2 and O_2 evolution and avoid the back reaction, showing quite stable performance during the gas evolution.

Conclusion

We report the chemically-driven RuO_2 nanowires and a facile method to fabricate three-dimensional RuO_2 branched Au-TiO_2 nanowire arrays for the photostable electrodes in PEC water oxidation. The amorphous RuO_2 precursors ($Ru(OH)_3{\cdot}H_2O$) are heated at 180 °C, producing the RuO_2 nanoparticles with the tetragonal crystallographic structure and Ru enriched amorphous phases, observed by the real time structural evolution during the growth process through the in-situ SXRD and the HRTEM images. Growth proceeds by Ru diffusion to the nanoparticles, followed by diffusion to the growing surface of the nanowire in oxygen ambient, supported by the nucleation theory. The RuO_2 branched Au-TiO_2 nanowire arrays shows a remarkable enhancement in the photocurrent density by approximately 60% and 200%, in the UV-visible and Visible region, respectively, compared with pristine TiO_2 nanowires at the same potential. Furthermore, there is no significant change in the device's photoconductance with UV-visible illumination during 1 day, making it possible to produce oxygen gas without the loss of the photoactivity. This may ascribe to the highly crystalline properties of the RuO_2 nanowires and means the good photostability of the designed electrode.

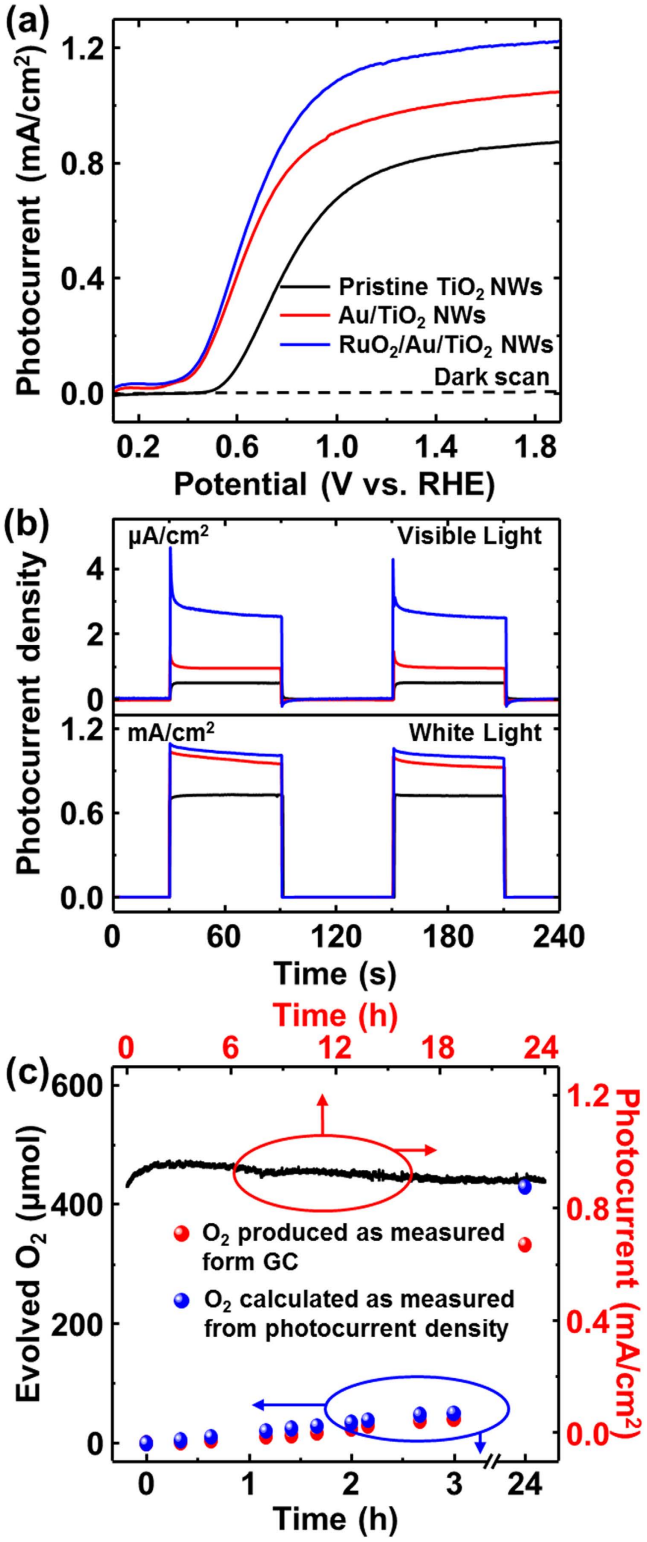

Figure 5. (**a**) Photocurrent versus potential characteristics of 0.5 M Na_2SO_4 (pH 7.2) electrolyte under AM 1.5 light illumination measured against the Ag/AgCl electrode with 30 mV/s scan rate. (**b**) Photocurrent density for chopped full spectrum (AM 1.5G) and visible illumination ($\lambda > 420$ nm long pass filter with AM 1.5G) at 1.62 V vs. RHE. (**c**) The quantity of evolved oxygen (red dots) measured (gas-chromatographically) as a function of time. The photocurrent simultaneously recorded with light illumination of white light (AM 1.5G) at 1.23 V vs. RHE.

Methods

Synthesis of RuO_2 nanowires and Growth Mechanism. Highly-crystalline RuO_2 nanowires were grown by a simple annealing process of the RuO_2 precursor via a simple reaction between $RuCl_3{\cdot}xH_2O$ and NaOH by carefully controlling pH (~9.00) of the aqueous solution at room temperature, as described previously[14]. This was found to be so simple and facile method for the growth of the nanowires. During this process, the amorphous RuO_2 precursor ($Ru(OH)_3{\cdot}H_2O$) were washed several times with deionized (DI) water to remove the remaining chlorides and sodium hydroxide, followed by the redispersion in DI water. For the detailed growth mechanism, it was spread on a Si (001) wafer and after drying at room temperature for 2 hrs, the sample are heated at the temperature ranging from 150 to 250 °C for 4 hrs.

Growth of 3D Branch-Shaped Nanostructure with Au nanoparticles. For the efficient oxygen production, TiO_2 nanowire arrays were first grown on fluorine-doped tin oxide (FTO) substrate by the hydrothermal method, reported elsewhere[32]. After washing with DI water, the sample was annealed in air at 450 °C for 4 hrs to improve the crystallinity of the nanowires. The AuNPs are formed by metal aggregation. The ~1 nm thick (mass thickness) Au film was then deposited on the TiO_2 nanowires using e-beam evaporation at a very slow deposition rate of less 0.1 Å/s and annealed at the temperature 250 °C for 1 min in nitrogen gas. The base pressure was maintained at 2.0×10^{-6} Torr. It produced well-separated AuNPs covering the nanowire uniformly. Finally, the RuO_2 precursor mixed in DI water (RuO_2 precursor are well-controlled from 3×10^{-6} to 6×10^{-4} wt%) are dropped into the sample and dried at 2 hrs, followed by the annealing process in atmosphere.

Microstructural analysis. The real time structural evolution during the growth process was done by the in-situ synchrotron radiation diffraction as the temperature increases to 150 ~ 600 °C, which was carried out at the 3D beamline at Pohang Accelerator Laboratory (PAL). For high-resolution XRD measurements, the wavelength of the incident X-ray was set at 1.488 Å by a double-bounce Si (111) monochromator. The SEM was done using a PHILIPS XL30S with an accelerating voltage of 5 kV. The HRTEM images were collected using a Cs-corrected JEM-2100 operated at 200 kV.

Photoelectrochemical Characterization. The PEC properties of the electrodes were studied in a three electrode cell with Ag/AgCl as the reference electrode and a Pt wire as the counter electrode. The working electrode area is in the range of ~0.2 cm^2. 0.5 M Na_2SO_4 aqueous solution (pH = 7.2) was used as an electrolyte for PEC measurements. Linear sweeps and time-profiled current generation were obtained by an IviumStat electrochemical analyzer, with Ag/AgCl as reference and Pt wire as counter electrode under simulated sunlight with a 150 W xenon lamp coupled with an AM 1.5 global filters (100 mW/cm^2). For visible light measurement, a long-wave pass filter ($\lambda > 430$ nm) was placed in front of the light source.

References

1. Kargar, A. *et al.* 3D Branched nanowire photoelectrochemical electrodes for efficient solar water splitting. *ACS Nano* **7,** 9407–9415 (2013).
2. Zhang, X., Liu, Y. & Kang, Z. 3D branched ZnO nanowire arrays decorated with plasmonic Au nanoparticles for high-performance photoelectrochemical water splitting. *ACS Appl. Mater. Interfaces*. **6,** 4480–4489 (2014).
3. Cho, I. S. *et al.* Branched TiO_2 nanorods for photoelectrochemical hydrogen production. *Nano Lett.* **11,** 4978–4984 (2011).
4. Lee, J.–H. Gas sensors using hierarchical and hollow oxide nanostructures: Overview. *Sens. Actuat. B* **140,** 319–336 (2009).
5. Ye, B. U. *et al.* Three-dimensional branched nanowire heterostructures as efficient light-extraction layer in light-emitting diodes. *Adv. Funct. Mater.* **24,** 3384–3391 (2014).
6. Kim, M. H. *et al.* Growth direction determination of a single RuO_2 nanowire by polarized Raman spectroscopy. *Appl. Phys. Lett.* **96,** 213108 (2010).
7. Chueh, Y.–L. *et al.* RuO_2 nanowires and RuO_2–TiO_2 core-shelled nanowires: from synthesis to mechanical, optical, electricaland photoconductive properties. *Adv. Mater.* **19,** 143–149 (2007).
8. Kudo, A. & Miseki, Y. Heterogeneous photocatalyst materials for water splitting. *Chem. Soc. Rev.* **38,** 253–278 (2009).
9. Tang, J. *et al.* Photoelectrochemical detection of glutathione by IrO_2–Hemin–TiO_2 nanowire arrays. *Nano Lett.* **13,** 5350–5354 (2013).
10. Mou, Z. *et al.* RuO_2/$TiSi_2$/graphene composite for enhanced photocatalytic hydrogen generation under visible light irradiation. *Phys. Chem. Chem. Phys.* **15,** 2793–2799 (2013).
11. Breault, T. M., Brancho, J. J., Guo, P. & Bartlett, B. M. Visible light water oxidation using a co-catalyst loaded anatase–structured $Ti_{1-(5x/4)}Nb_xO_{2-y-\delta}N_y$ Compound. *Inorg. Chem.* **52,** 9363–9368 (2013).
12. Jin, J. *et al.* Exploration of the interaction of RuO_2–Au composite nanoparticles formed by one-step synthesis within the mesopores. *Chem. Mater.* **25,** 3921–3927 (2013).
13. InvestmentMine, 5 Year Ruthenium Prices and Price Charts, http://www.infomine.com/investment/metal-prices/ruthenium/5-year/, accessed: August, 2014.
14. Lee, Y. *et al.* Facile synthesis of single crystalline metallic RuO_2 nanowires and electromigration-induced transport properties. *J. Phys. Chem. C* **115,** 4611–4615 (2011).
15. Chen, Z. G., Pei, F., Pei, Y. T. & De Hosson, J. T. M. A versatile route for the synthesis of single crystalline oxide nanorods: Growth behavior and field emission characteristics. *Cryst. Growth Des.* **10,** 2585–2590 (2010).
16. Yao, B. D., Chan, Y. F. & Wang, N. Formation of ZnO nanostructures by a simple way of thermal evaporation. *Appl. Phys. Lett.* **81,** 757–759 (2002).
17. Dai, Z. R., Pan, Z. W. & Wang Z. L. Novel nanostructures of functional oxides synthesized by thermal evaporation. *Adv. Funct. Mater.* **13,** 9–24 (2003).

18. Shrestha, K. M., Sorensen, C. M. & Klabunde, K. J. Synthesis of CuO nanorods, reduction of CuO into Cu nanorods, and diffuse reflectance measurements of CuO and Cu nanomaterials in the near infrared region. *J. Phys. Chem. C* **114,** 14368–14376 (2010).
19. Chen, J. T. *et al.* CuO nanowires synthesized by thermal oxidation route. *J. Alloy Comp.* **454,** 268–273 (2008).
20. Kim, M. H. *et al.* Growth of metal oxide nanowires from supercooled liquid nanodroplets. *Nano Lett.* **9,** 4138–4146 (2009).
21. Takahashi, K., Limmer, S. J., Wang, Y. & Cao, G. Synthesis and electrochemical properties of single-crystal V_2O_5 nanorod arrays by template-based electrodeposition. *J. Phys. Chem. B* **108,** 9795–9800 (2004).
22. Liu, J. *et al.* Enhanced field emission properties of MoO_2 nanorods with controllable shape and orientation. *Mater. Lett.* **58,** 3812–3815 (2004).
23. Cai, L., Rao, P. M. & Zheng, X. Morphology-controlled flame synthesis of single, branched, and flower-like α-MoO_3 nanobelt arrays. *Nano Lett.* **11,** 872–877 (2011).
24. Duvigneaud, P. H. & Reinhard-Deire, D. DTA study of RuO_2 formation from the thermal decomposition of ruthenium(III) hydrate. *Thermochim. Acta* **51,** 307–314 (1981).
25. Kim, Y. D., Schwegmann, S., Seitsonen, A. P. & Over, H. Epitaxial growth of RuO_2(100) on Ru(10$\bar{1}$0): Surface structure and other properties. *J. Phys. Chem. B* **105,** 2205–2211 (2001).
26. O'Neill, H. S. C. & Nell, J. Gibbs free energies of formation of RuO_2, lrO_2, and OsO_2: A high-temperature electrochemical and calorimetric study. *Ceochim. Cosmochim. Acta* **61,** 5279–5293, (1997).
27. Barin, I. *Thermochemical data of pure substances* [1254] (Wiley, New York, 1989).
28. Pu, Y.–C. *et al.* Au nanostructure-decorated TiO_2 nanowires exhibiting photoactivity across entire UV-visible region for photoelectrochemical water splitting. *Nano Lett.* **13,** 3817–3823 (2013).
29. Li, J. *et al.* A three-dimensional hexagonalfluorine-doped tin oxide nanocone array: a superior light harvesting electrode for high performance photoelectrochemical water splitting. *Energy Environ. Sci.* **7,** 3651–3658 (2014).
30. Li, X. Z., He, C., Graham, N. & Xiong, Y. Photoelectrocatalytic degradation of bisphenol A in aqueous solution using a Au–TiO_2/ITO film. *J. Appl. Electrochem.* **35,** 741–750 (2005).
31. T. Hisatomi, J. Kubota & K. Domen, Recent advances in semiconductors for photocatalytic and photoelectrochemical water splitting, *Chem. Soc. Rev.* **43,** 7520–7535 (2014).
32. Liu, B. & Aydil, E. S. Growth of oriented single-crystalline rutile TiO_2 nanorods on transparent conducting substrates for dye-sensitized solar cells. *J. Am. Chem. Soc.* **131,** 3985–3990 (2009).

Acknowledgements

This work was supported the Pioneer Research Center Program (2013M3C1A3063602) of the National Research Foundation of Korea (NRF) grant funded by the Ministry of Science, ICT & Future Planning (MSIP), and by Basic Science Program through the National Research Foundation of Korea (NRF) funded by MEST (Nos. 2014R1A1A2059791 for MHK). This work was also financially supported by the KIST-UNIST partnership program (2V03870/2V03880) and equivalently by the 2014 Research Fund (1.140019.01) of UNIST (Ulsan National Institute of Science and Technology). We are very thankful to Prof. Suk-Bin Lee (UNIST) for great contribution in this paper.

Author Contributions

J.P., J.W.L., B.U.Y. and S.H.C. performed the experiments and analyzed the data. H.Y.J. performed the TEM experiments. H.P., S.H.J. and H.L. revised the manuscript. J.M.B. and M.H.K. conceived of and supervised this study, and provided intellectual and technical guidance. All authors discussed the results, wrote and commented on the manuscript.

Additional Information

Supplementary information accompanies this paper at http://www.nature.com/srep

Competing financial interests: The authors declare no competing financial interests.

How to cite this article: Park, J. *et al.* Structural Evolution of Chemically-Driven RuO_2 Nanowires and 3-Dimensional Design for Photo-Catalytic Applications. *Sci. Rep.* **5**, 11933; doi: 10.1038/srep11933 (2015).